# Degradation of Terrigenous Dissolved Organic Carbon in the Western Arctic Ocean

Dennis A. Hansell, *et al.*

*Science* **304**, 858 (2004);
DOI: 10.1126/science.1096175



*Science* (print ISSN 0036-8075; online ISSN 1095-9203) is published weekly, except the last week in December, by the American Association for the Advancement of Science, 1200 New York Avenue NW, Washington, DC 20005. 

perovskite phase suggests slow longitudinal elastic-wave velocities propagating along the [010] direction. In addition, it is also inferred that the post-perovskite phase forms a platy crystal habit parallel to the (010) plane as a result of the sheet-stacking structure. A strong preferred orientation of such platy crystals may develop under the shear flow. A large *S*-wave polarization anisotropy ($V_{SH} > V_{SV}$) observed in the D″ region (*1*, *2*) is possibly caused by the preferred orientation of the post-perovskite phase with the (010) plane being parallel to the horizontal shear flow, which is introduced by the downwelling of slabs and upwelling of plumes. This also provides an explanation for seismic anisotropy that is found only below the D″ discontinuity in the deep lower mantle.


**References and Notes**

1. B. J. Mitchell, D. V. Helmberger, *J. Geophys. Res.* **78**, 6009 (1973).
2. T. Lay, D. V. Helmberger, *Geophys. J. R. Astron. Soc.* **75**, 799 (1983).
3. M. E. Wysession *et al.*, in *The Core-Mantle Boundary Region*, M. Gurnis, M. E. Wysession, E. Knittle, B. A. Buffet, Eds. (American Geophysical Union, Washington, DC, 1998), vol. 28, pp. 273–297.
4. I. Sidorin, M. Gurnis, D. V. Helmberger, *Science* **286**, 1326 (1999).
5. E. Knittle, R. Jeanloz, *Science* **235**, 668 (1987).
6. G. Serghiou, A. Zerr, R. Boehler, *Science* **280**, 2093 (1998).
7. G. Fiquet, A. Dewaele, D. Andrault, M. Kunz, T. Le Bihan, *Geophys. Res. Lett.* **27**, 21 (2000).
8. R. M. Wentzcovitch, J. L. Martins, G. D. Price, *Phys. Rev. Lett.* **70**, 3947 (1993).
9. L. Stixrude, R. E. Cohen, *Nature* **364**, 613 (1993).
10. M. C. Warren, G. J. Ackland, B. B. Karki, S. J. Clark, *Mineral. Mag.* **62**, 585 (1998).
11. S. H. Shim, T. S. Duffy, G. Shen, *Science* **293**, 2437 (2001).
12. C. Meade, H. K. Mao, J. Hu, *Science* **268**, 1743 (1995).
13. S. K. Saxena *et al.*, *Science* **274**, 1357 (1996).
14. H. K. Mao, G. Shen, R. J. Hemley, *Science* **278**, 2098 (1997).
15. XRD spectra were collected on an imaging plate with an exposure time of 1 to 5 min. A monochromatic incident x-ray beam with a wavelength of 0.4134 or 0.4136 Å was collimated to 20 μm in diameter. The two-dimensional XRD image was integrated as a function of 2θ in order to give a conventional one-dimensional diffraction profile.
16. M. Murakami, K. Hirose, S. Ono, Y. Ohishi, *Geophys. Res. Lett.* **30**, 11 (2003).
17. S. Ono, K. Hirose, M. Isshiki, K. Mibe, Y. Saito, *Phys. Chem. Miner.* **29**, 527 (2002).
18. G. Shen, H. K. Mao, R. J. Hemley, in *Proceedings of the 3rd NIRIM International Symposium on Advanced Materials* (National Institute for Research in Inorganic Materials, Tsukuba, Japan, 1996), pp. 149–152.
19. T. Watanuki, O. Shimomura, T. Yagi, T. Kondo, M. Isshiki, *Rev. Sci. Instrum.* **72**, 1289 (2001).
20. J. C. Jamieson, J. N. Fritz, M. H. Manghnani, in *High Pressure Research in Geophysics*, S. Akimoto, M. H. Manghnani, Eds. (Reidel, Boston, 1982).
21. S. H. Shim, T. S. Duffy, G. Shen, *Phys. Earth Planet. Int.* **120**, 327 (2000).
22. T. Uchida, N. Funamori, K. Oguri, Y. Nakamura, T. Yagi, *Rev. High Press. Sci. Technol.* **5**, 261 (1996).
23. D. H. Xiong, L. C. Ming, M. H. Manghnani, *Phys. Earth Planet. Int.* **43**, 244 (1986).
24. The MD calculations were carried out with the full Ewald method for electrostatic interactions, the velocity Verlet algorithm with a 2-fs time step for integration of equations of motions of atoms, and constant number of atoms-volume-temperature (NVT) and constant number of atoms-temperature-pressure (NTP) ensembles. The interatomic potential model used in the calculation was prepared to well reproduce the perovskite-type $MgSiO_3$ structure at 300 K (observed $a = 4.325$ Å, $b = 4.579$ Å, and $c = 6.308$ Å; calculated $a = 4.403$ Å, $b = 4.574$ Å, and $c = 6.410$ Å at 109 GPa).
25. G. Fiquet *et al.*, *Phys. Earth Planet. Int.* **105**, 21 (1998).
26. P. H. Noël, J. Padiou, *Acta Crystallogr.* **B32**, 1593 (1976).
27. I. Sidorin, M. Gurnis, D. V. Helmberger, *J. Geophys. Res.* **104**, 15005 (1999).
28. G. Masters, D. Gubbins, *Phys. Earth Planet. Int.* **140**, 159 (2003).
29. Y. Fei, *Am. Mineral.* **84**, 272 (1999).


30. We thank Y. Tatsumi, T. Tsuchiya, D. Yuen, J. Tuff, and Y. Kuwayama for discussions. In situ x-ray measurements were conducted at SPring-8 (proposal no. 2002B0537-ND2-np and 2003A0013-LD2-np). M.M. was supported by the Japan Society for the Promotion of Science (JSPS) Research Fellowships for Young Scientists.


**Supporting Online Material**

www.sciencemag.org/cgi/content/full/1095932/DC1
Figs. S1 and S2
Table S1


22 January 2004; accepted 29 March 2004
Published online 8 April 2004; 10.1126/science.1095932
Include this information when citing this paper.


# Degradation of Terrigenous Dissolved Organic Carbon in the Western Arctic Ocean


**Dennis A. Hansell,[1]* David Kadko,[1] Nicholas R. Bates[2]**



**The largest flux of terrigenous organic carbon into the ocean occurs in dissolved form by way of rivers. The fate of this material is enigmatic; there are numerous reports of conservative behavior over continental shelves, but the only knowledge we have about removal is that it occurs on long unknown time scales in the deep ocean. To investigate the removal process, we evaluated terrigenous dissolved organic carbon concentration gradients in the Beaufort Gyre of the western Arctic Ocean, which allowed us to observe the carbon's slow degradation. Using isotopic tracers of water-mass age, we determined that terrigenous dissolved organic carbon is mineralized with a half-life of 7.1 ± 3.0 years, thus allowing only 21 to 32% of it to be exported to the North Atlantic Ocean.**


Terrigenous dissolved organic carbon (tDOC) enters the global ocean by way of rivers at a rate of ~0.25 Pg C $yr^{-1}$ (*1*), constituting the largest transfer of reduced carbon from the continents to the open ocean. The fate of this material once it is delivered to the ocean remains uncertain. Studies that use salinity-DOC relationships across the world's estuaries and ocean margins show conservative tDOC behavior (*1*, *2*), suggesting a long-lived material. In contrast, low concentrations of tDOC tracers in the open ocean (e.g., lignin and stable isotopic compositions) (*3*, *4*) indicate active removal processes, but the time and space scales of the processes remain unknown.

On a per volume basis, the Arctic Ocean receives the greatest loads of terrestrial fresh water and organic matter of any ocean. Rivers draining into the Arctic Ocean comprise ~10% of the global river flux and have high DOC content (*5*), typically >600 μM C. This material is long lived, such that up to ~25% of the DOC in the surface central Arctic consists of terrigenous components (*6*, *7*). Previous studies that have used DOC-salinity relationships in the eastern Arctic Ocean (e.g., the Eurasian Basin and its bordering seas) have indicated that tDOC in fluvial water mixes conservatively with marine water over the continental margins (*8*, *9*), yet <50% of the tDOC entering the Arctic Ocean survives for export to the North Atlantic (*6*, *10*).

The gyre circulation of the western Arctic Ocean (i.e., the Canada Basin and adjacent continental shelf seas) provides the conditions necessary for observing substantial tDOC removal over decadal time scales. In this study, physical and biogeochemical measurements were made from the *USCGC Healy* during a spring cruise (5 May to 15 June 2002; sea-ice cover >90%) to the Chukchi Sea as part of the Western Arctic Shelf-Basin Interactions (SBI) project (*11*). Thirty-nine stations, largely on three meridional sections, were occupied on the Chukchi Sea shelf and in the adjacent Arctic Ocean basin (Fig. 1). The parts of the sections that are located over the continental shelf largely comprised water of Pacific Ocean origin (by way of the Bering Strait). Present at the northern end of the sections, over the deep Canada Basin, was the polar surface layer (PSL), an ice-covered, relatively low-salinity water mass that is a mix of riverine waters (~8 m of meteoric water in the upper 40 m) (*12*) and marine waters (*13*). The upper few hundred meters of the Arctic Ocean are strongly strati-


[1]Rosenstiel School of Marine and Atmospheric Science, University of Miami, Miami, FL 33149, USA. [2]Bermuda Biological Station for Research, 17 Biological Lane, Ferry Reach, St. George's GE-01, Bermuda.

*To whom correspondence should be addressed. E-mail: dhansell@rsmas.miami.edu

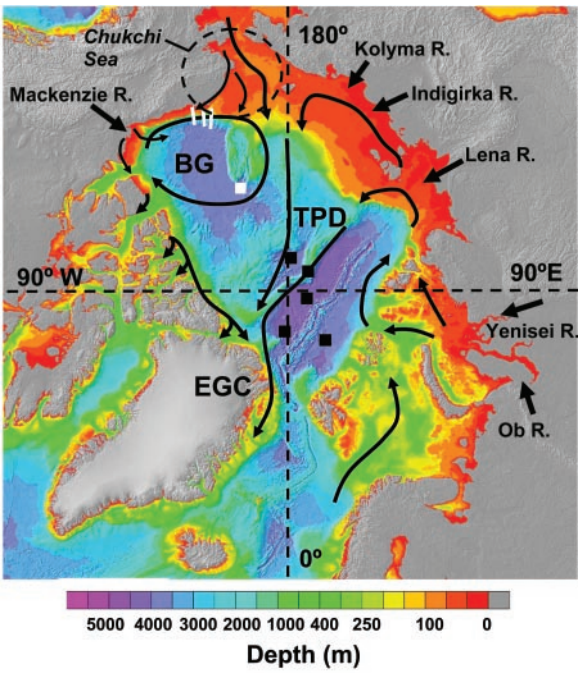


**Fig. 1.** Bathymetric map of the Arctic (*29*) with schematic representation of surface ocean circulation. The locations of the mouths of the major rivers draining into the Arctic Ocean are indicated. Locations of sampling sites for determination of the $^{228}Ra/^{226}Ra$ ratios in the Transpolar Drift (TPD) and at Ice Station T3 are indicated by black and white squares, respectively. The nominal locations of the sections occupied in this work are shown as three white lines at the edge of the Beaufort Gyre (BG), located over the Canada Basin. The location of the Chukchi Sea is indicated by the dashed circle. The East Greenland Current (EGC) is indicated.

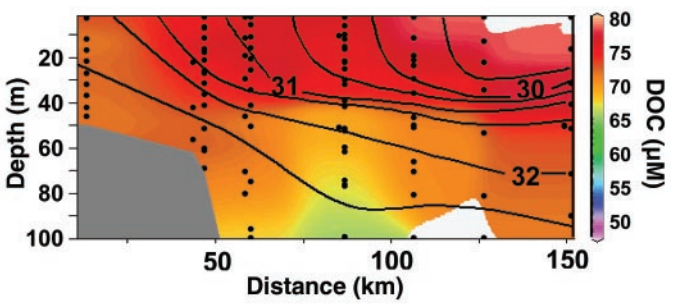


**Fig. 2.** Distributions of DOC (shown by color contours in μM) and salinity (lined contours) in the upper 100 m on the westernmost meridional section of the SBI program. Location is indicated in Fig. 1.

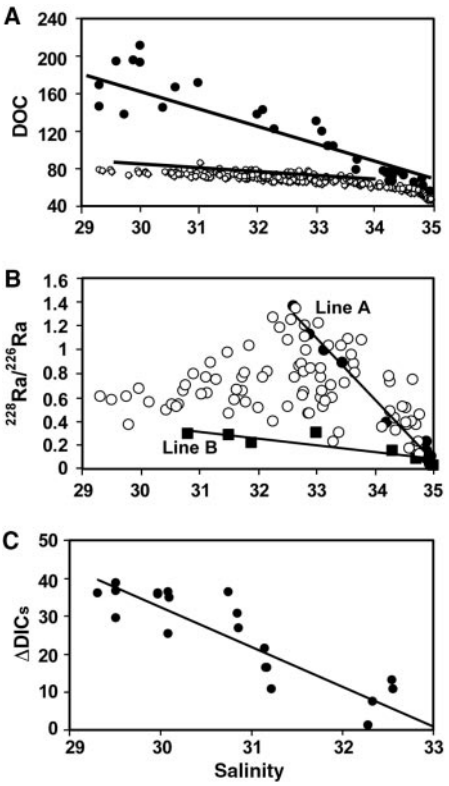


**Fig. 3.** Property/property plots of salinity versus relevant variables. (**A**) DOC data are shown from this study (open circles; DOC = –2.60 × salinity + 154; $R^2 = 0.39$; $N = 96$) and, for comparison, from published data from the Eurasian Arctic (*30*) [solid circles; DOC = –14.82 × salinity + 596; $R^2 = 0.98$; $N = 25$ (*30*)]. Regression of the western Arctic data are for data pairs at salinity <33.5; higher salinity data are from the deeper Atlantic layer. (**B**) $^{228}Ra/^{226}Ra$ data, taken from published accounts, are from the Transpolar Drift (*21*) (solid circles, Line A) and from Ice Station T3 (squares, Line B) in the Beaufort Gyre (*22*). $^{228}Ra/^{226}Ra$ ratios (open circles) measured during SBI in spring 2002 are from the sections shown in Fig. 1 at the Chukchi shelf break. The SBI $^{228}Ra/^{226}Ra$ ratios fall approximately between Lines A and B. (**C**) $\Delta DIC_s$ is a measure of the accumulation of DIC due to tDOC mineralization, corrected for mixing. $\Delta DIC_s$ is estimated from the relationship between DIC and salinity observed during the spring SBI program in 2002. The marine end member in the PSL (i.e., Pacific Ocean water at a salinity of 32.5) has a DIC concentration of ~2150 to 2160 μmol $kg^{-1}$. Given the DIC concentration of sea-ice melt water (~0 μmol $kg^{-1}$) and fresh water (~100 μmol $kg^{-1}$), a plot of DIC versus salinity would have a regression of 66.28 × salinity – 4.336. However, the observed DIC versus salinity relationship has a regression of 55.802 × salinity – 342.4 (zero-salinity intercept of 342.4 μmol $kg^{-1}$). The deviation between the two mixing regressions ($\Delta DIC_s$ = –10.48 × salinity + 346.7; black line) indicates accumulation of DIC in the Beaufort Gyre, corrected for mixing (i.e., an observed accumulation of ~10.5 μM DIC per unit salinity decrease in the PSL).

fied. Immediately beneath the PSL are the upper halocline waters (UHW) (depth of ~40 to 120 m, core-layer salinity of 33.1) of Pacific Ocean origin and the lower halocline waters (depth of ~130 to 220 m, core-layer salinity of 34.3) of Atlantic Ocean origin.

The Pacific Ocean is the primary source of marine water to the PSL and UHW (~2.5 × $10^4$ $km^3$ $yr^{-1}$ through the Bering Strait) of the western Arctic Ocean, and the Mackenzie and Lena Rivers are the largest sources of fresh water (249 and 524 $km^3$ $yr^{-1}$, respectively) (*5*). The PSL and UHW over the Canada Basin circulate within the anticyclonic Beaufort Gyre (Fig. 1), facilitating long-term retention of those waters. The circulation and composition of the PSL in the eastern Arctic differ considerably from the western Arctic Ocean. In the east, the Atlantic Ocean serves as the primary marine source and eastern Eurasian rivers dominate as the freshwater source (Fig. 1). Eurasian shelf and river water are transported across the Arctic Ocean in the Transpolar Drift (*14*–*16*) and exported to the North Atlantic by way of the East Greenland Current. The absence of a large-scale gyre circulation in the east precludes the long-term retention of the PSL that is found in the western Arctic Ocean, thus constituting the salient circulation difference between the two systems.

Concentrations of total DOC (marine plus terrigenous) and salinity in the upper 100 m of the westernmost SBI transect are shown in Fig. 2. In the surface layer (0 to 40 m), salinity decreased from >32 on-shelf to <30 in the PSL, whereas DOC had the opposite trend, increasing from ~70 μM on-shelf to ~80 μM over the basin. These data indicate that Pacific Ocean water of moderate salinity and DOC is present on the Chukchi Sea shelf and that PSL water with lower salinity and higher DOC (the riverine contribution) (*6*, *7*) is present over the deep basin. Underlying the PSL (Fig. 2; at depths of >40 m), Pacific Ocean water that had been transported off the continental shelf was present as UHW. Below this layer were lower halocline and Atlantic waters characterized by higher salinities (>34) and lower DOC concentrations (<60 μM) (Fig. 3A).

Plots of DOC versus salinity provide insights on the relationship between Arctic Ocean hydrography and tDOC (*8*, *9*, *17*, *18*). Data from the SBI field study as well as data repre-

sentative of the eastern Arctic Ocean are shown together in Fig. 3A. Both data sets demonstrate linear mixing between fresher, higher DOC water and marine, lower DOC water [in the case of the SBI data, mixing is between high-DOC PSL water (salinity <30) and low-DOC Pacific Ocean water (salinity 33 to 34)]. The prominent difference between the data sets is the tDOC concentrations in the freshwater end members (zero-salinity intercepts of the *y* axis). In the eastern Arctic, the intercept indicates a tDOC concentration (±SD) of 596 ± 9 μM (Fig. 3A). This value is similar to the discharge-weighted mean DOC concentration in the major rivers draining into the eastern Arctic shelf seas, suggesting that the tDOC is conservatively mixed into Arctic Ocean basin waters. In contrast, the zero-salinity intercept in the western Arctic Ocean is 154 ± 7 μM, or 442 ± 11 μM lower than in the eastern Arctic.

The difference in the zero-salinity intercepts suggests substantial removal of tDOC in the western Arctic Ocean. To evaluate the quantity of removal, the concentration of tDOC in the western Arctic rivers entering the PSL of the Beaufort Gyre must be established. The discharge-weighted mean DOC concentration in the major rivers draining into western Arctic shelf seas (Laptev, East Siberian, Chukchi, and Beaufort Seas) is ~540 μM (*19*). The Lena and Mackenzie Rivers (Fig. 1) dominate the western Arctic Ocean tDOC budget, together representing 83% of the $6 \times 10^{12}$ gC $yr^{-1}$ tDOC discharge into the Canada Basin (*5*). The Lena River, adding $3.4 \times 10^{12}$ gC $yr^{-1}$ as tDOC to the Arctic Ocean, has a reported tDOC concentration of ~538 μM (*5*). The concentrations of tDOC in the Mackenzie River (adding $1.9 \times 10^{12}$ gC $yr^{-1}$), the major source of fresh water in the southern sector of the Beaufort Gyre (*12*), appear to be more variable (360 to 730 μM) (*5*). A survey (from 1993) of DOC in Mackenzie River tributaries during the summer, when most of the river discharge occurs and tDOC concentrations are highest, indicated a tDOC value of 550 ± 122 μM (*20*). Here, a value of 550 ± 100 μM (similar to concentrations measured in both the Lena and Mackenzie Rivers) (*5*, *20*) is taken as representative of the tDOC concentration in the western Arctic rivers. With this value as the initial tDOC concentration, the zero-salinity tDOC intercept of 154 ± 7 μM in the PSL indicates the removal of 396 ± 50 μM tDOC in the PSL of the Canada Basin.

The half-life of tDOC in the western Arctic Ocean has been determined with the use of the ratio $^{228}Ra/^{226}Ra$ as an age tracer. The $^{228}Ra/^{226}Ra$ ratio of seawater is a valuable tracer for water masses because it provides information about the time since water masses were last in contact with the continental shelf (*21*). High $^{228}Ra/^{226}Ra$ ratios were reported in the Transpolar Drift near the North Pole (Fig. 3B), indicating rapid transport (<3 years elapsed time) of surface water from the Eurasian and Siberian shelves into the central Arctic Ocean (*21*). In contrast, low $^{228}Ra/^{226}Ra$ ratios in the surface Beaufort Gyre at Ice Station T3 (*22*) (Fig. 3B) indicate a much longer residence time of ~20 years (*21*). These residence times for the Transpolar Drift and the Beaufort Gyre bracket the average residence times of river water in the surface Arctic that have previously been reported [11 to 15 years for the entire surface Arctic Ocean (*16*) and 4.1 to 6.5 years for the riverine component of the PSL in the Eurasian Basin (*15*)].

The $^{228}Ra/^{226}Ra$ ratios measured during the SBI field study at the Chukchi Sea shelf break (Fig. 3B) largely fall between the ratios defined by the Transpolar Drift radium data (Line A, young water) and by the Beaufort Gyre data at Ice Station T3 (Line B, aged water). The SBI data indicate three end members: (i) high salinity (34 to 35), low $^{228}Ra/^{226}Ra$ ratio (old) Atlantic water; (ii) intermediate salinity (32.5 to 33.5), high $^{228}Ra/^{226}Ra$ ratio (young) Pacific Ocean water, having recently transited through the shallow Bering Strait; and (iii) low salinity (<31), intermediate $^{228}Ra/^{226}Ra$ ratio (aged) PSL (Fig. 3B). The surface water $^{228}Ra/^{226}Ra$ ratios measured on the westernmost SBI section (Fig. 4) showed the anticipated on-to-off–shelf decrease in ratio. There was a steep horizontal gradient in age, from 0 to 1 years over the shelf to 13 ± 1 years for PSL waters sampled at the southern edge of the Beaufort Gyre (Fig. 4), indicating the long residence time of water in the gyre. With a 396 ± 50 μM decrease in the tDOC concentration over that period, a tDOC half-life of 7.1 ± 3.0 years and a tDOC decay constant of 0.097 ± 0.004 $yr^{-1}$ were calculated.

Comparison of the western Arctic Ocean DOC-salinity relationship (Fig. 3A; slope = –2.6) with that expected from conservative mixing of western Arctic marine and river waters (slope = –14.7) indicates a cumulative loss of ~12.1 μM of tDOC per unit salinity decrease. Microbial degradation of tDOC to its mineralization product $CO_2$ should manifest itself as the accumulation of dissolved inorganic carbon (DIC) in the upper ocean layer (air-sea $CO_2$ gas exchange and vertical diffusion rates are low due to year-long sea-ice cover and low vertical-diffusivity rates). We observed an accumulation of ~10.5 μM of DIC per unit salinity decrease (or 87% of the tDOC decrease) in the PSL relative to that expected from freshening of Pacific Ocean source water by ice melt and fresh water (Fig. 3C legend). The mass balance for carbon (△DIC ≈ △tDOC) suggests that microbial degradation predominates as the tDOC removal mechanism.

Given the average residence time of river water in the surface Arctic of 11 to 15 years (*16*) [or the modeled mean Arctic river water travel time to Fram Strait of 12 to 14 years (*15*)] and the tDOC decay constant determined here, the $15 \times 10^{12}$ gC of tDOC annually entering the Arctic Ocean (*5*) will be reduced to between $3.2 \times 10^{12}$ and $4.9 \times 10^{12}$ gC (21 to 32% of input) before its subsequent export to the North Atlantic. In comparison, analysis of DOM fluorescence indicated that 20 to 50% of Arctic tDOC is exported in the East Greenland Current (*10*), the major conduit of upper-layer Arctic water to the North Atlantic, whereas lignin analysis (*6*) indicated that 12 to 41% is exported there.

Understanding the processes that control either the degradation of tDOC (internal to the Arctic Ocean) or its preservation (ultimately with export to the North Atlantic Ocean) is a critical issue, particularly in light of the recent changes in the hydrological cycle of the Arctic region. More than half of the global storage of organic carbon in soils is found in the Arctic drainage areas (*23*), though at present much of the tDOC delivered to the Arctic Ocean is of modern age (*24*). Increased Arctic river runoff (*25*) is likely to change the flux of organic carbon into the Arctic Ocean, and contemporaneous changes in the system's circulation (*26*), summertime sea-ice cover and extent (*27*)

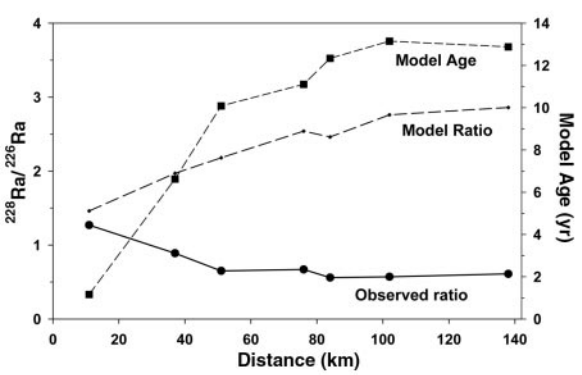


**Fig. 4.** $^{228}Ra/^{226}Ra$ ratios and derived water-mass ages. Observed and model ratios [the latter given no loss of $^{228}Ra$ by radioactivity (zero-age)] as well as the model ages of surface water (depth of 7 m) are shown along the westernmost section sampled (Fig. 1). The expected $^{228}Ra/^{226}Ra$ ratio on the section, given no radioactive decay (zero-age water), was modeled as a function of salinity derived from Line A in Fig. 3B (thus accounting for rapid offshore mixing, as was done in aging the water of the Transpolar Drift) (*21*). The apparent ages of the water were determined by comparing the modeled zero-age ratios to the observed ratios.

(impacting the potential for tDOC photooxidation), and water column stability and halocline development (*28*) will likely change the residence time and hence the fate of tDOC in the region. Further insights developed on the processes of tDOC removal in the Arctic will advance our understanding of tDOC sinks at lower latitudes, where the majority of the tDOC enters the global ocean.

### References and Notes


1. G. Cauwet, in *Biogeochemistry of Marine Dissolved Organic Matter*, D. A. Hansell, C. A. Carlson, Eds. (Academic Press, San Diego, CA, 2002), pp. 579–609.
2. R. F. C. Mantoura, E. M. S. Woodward, *Geochim. Cosmochim. Acta* **47**, 1293 (1983).
3. S. Opsahl, R. Benner, *Nature* **386**, 480 (1997).
4. J. I. Hedges, R. G. Keil, R. Benner, *Org. Geochem.* **27**, 195 (1997).
5. L. G. Anderson, in *Biogeochemistry of Marine Dissolved Organic Matter*, D. A. Hansell, C. A. Carlson, Eds. (Academic Press, San Diego, CA, 2002), pp. 665–683.
6. S. Opsahl, R. Benner, R. M. W. Amon, *Limnol. Oceanogr.* **44**, 2017 (1999).
7. P. A. Wheeler, J. M. Watkins, R. L. Hansing, *Deep-Sea Res. II* **44**, 1571 (1997).
8. R. M. W. Amon, in *The Arctic Ocean Organic Carbon Cycle*, R. Stein, R. W. Macdonald, Eds. (Springer, New York, 2003), pp. 83–99.
9. G. Kattner *et al.*, *Mar. Chem.* **65**, 25 (1999).
10. R. M. W. Amon, G. Budeus, B. J. Meon, *J. Geophys. Res.* **108**, 3221, 10.1029/2002JC001594 (2003).
11. J. Grebmeier, *Arct. Res. U.S.* **17**, 24 (2003).
12. R. W. Macdonald, F. A. McLaughlin, E. C. Carmack, *Deep-Sea Res. I* **49**, 1769 (2002).
13. K. Aagaard, E. C. Carmack, *J. Geophys. Res.* **94**, 14485 (1989).
14. C. K. H. Guay *et al.*, *J. Geophys. Res.* **106**, 11469 (2001).
15. M. J. Karcher, J. M. Oberhuber, *J. Geophys. Res.* **107**, 10.1029/2000JC000530 (2002).
16. D. Bauch, P. Schlosser, R. G. Fairbanks, *Prog. Oceanogr.* **35**, 53 (1995).
17. A. Fransson *et al.*, *Cont. Shelf Res.* **21**, 225 (2001).
18. C. K. H. Guay *et al.*, *Geophys. Res. Lett.* **26**, 1007 (1999).
19. J. M. Lobbes, H. P. Fitznar, G. Kattner, *Geochim. Cosmochim. Acta* **64**, 2973 (2000).
20. I. G. Droppo, D. Jeffries, C. Jaskot, S. Backus, *Arctic* **51**, 155 (1998).
21. M. M. Rutgers van der Loeff, R. M. Key, J. Scholten, D. Bauch, A. Michel, *Deep-Sea Res. II* **42**, 1533 (1995).
22. A. Kaufman, R. M. Trier, W. S. Broecker, H. W. Feely, *J. Geophys. Res.* **78**, 8827 (1973).
23. T. Dittmar, G. Kattner, *Mar. Chem.* **83**, 103 (2003).
24. R. Benner, B. Benitez-Nelson, R. M. W. Amon, *Geophys. Res. Lett.* **31**, L05305, 10.1029/2003GL019251 (2004).
25. B. J. Peterson, R. M. Holmes, J. W. McClelland, C. J. Voeroesmarty, *Science* **298**, 2171 (2002).
26. A. Y. Proshutinsky, M. A. Johnson, *J. Geophys. Res.* **102**, 12493 (1997).
27. C. Deser, J. E. Walsh, M. S. Timlin, *J. Clim.* **13**, 617 (2000).
28. M. Steele, T. Boyd, *J. Geophys. Res.* **103**, 10419 (1998).
29. The bathymetric map of the Arctic Ocean was prepared by M. Jakobsson, N. Z. Cherkis, J. Woodward, R. Mcnab, and B. Coakley, and is available at www.ngdc.noaa.gov/mgg/bathymetry/arctic/currentmap.html.


30. R. M. W. Amon, R. Benner, *Deep-Sea Res. I* **50**, 151 (2003).
31. Supported by the Arctic System Science Program, Office of Polar Programs, NSF (OPP-0124900, OPP-0124872, and OPP-0124868). We thank the crew and officers of the *USCGC Healy* as well as our SBI colleagues for their assistance in the collection of our data.

29 January 2004; accepted 31 March 2004


# Old World Fossil Record of Modern-Type Hummingbirds

**Gerald Mayr**

**I report on tiny skeletons of stem-group hummingbirds from the early Oligocene of Germany that are of essentially modern appearance and exhibit morphological specializations toward nectarivory and hovering flight. These are the oldest fossils of modern-type hummingbirds, which had not previously been reported from the Old World. The findings demonstrate that early hummingbird evolution was not restricted to the New World. They further suggest that bird–flower coevolution dates back to the early Oligocene and open another view on the origin of ornithophily in Old World plants.**

Today's hummingbirds (Apodiformes, Trochilidae) exclusively occur in the New World. Little is known about their early evolution (*1*), and the fossil record of the crown group, the clade that includes the stem species of the modern taxa and its descendants, is exceedingly poor, consisting of a small number of bones from the Quaternary of Central America (*2*, *3*). Although some apodiform birds from the early Tertiary of Europe and Asia were recently shown to be stem-group hummingbirds, i.e., hummingbirds outside the crown group (*4*), these are either very different from the modern taxa (*5*, *6*) or known from a few wing elements only (*7*). Here, I describe a taxon of stem-group hummingbirds from the early Oligocene of Germany that is of essentially modern appearance and exhibits morphological specializations toward nectarivory and hovering flight.

Forschungsinstitut Senckenberg, Division of Ornithology, Senckenberganlage 25, D-60325 Frankfurt a.M., Germany. E-mail: Gerald.Mayr@senckenberg.de

The classification of the species is Aves Linnaeus, 1758; Apodiformes Peters, 1940; Trochilidae Vigors, 1825; *Eurotrochilus inexpectatus* gen. et sp. nov. **Holotype.** SMNS (Staatliches Museum für Naturkunde, Stuttgart, Germany) 80739/4, partial disarticulated skeleton (Fig. 1). **Referred specimen.** SMNS 80739/3a+b, partial disarticulated skeleton on two slabs (Fig. 2). **Etymology**. *Euro*, for Europe, and *Trochilus*, the type genus of modern Trochilidae. The specific name is derived from Latin *inexpectatus* for unexpected and refers to the surprising occurrence of modern-type hummingbirds in Europe. **Type locality and horizon.** Frauenweiler south of Wiesloch (Baden-Württemberg, Germany), clay pit of the Bott-Eder GmbH ("Grube Unterfeld"); Rupelian, early Oligocene (30 to 34 million years ago) (*8–10*).

**Diagnosis.** *Eurotrochilus inexpectatus* is differentiated from all avian taxa except

**Table 1.** Length measurements and ratios of skeletal elements of fossil and extant hummingbirds. Measurements are given in millimeters; *P. pretrei*, *G. hirsuta*, and *C. mosquitus* are extant taxa.

| | Humerus | Ulna | Carpometacarpus | Tibiotarsus | Tarsometatarsus | Sternum | Sternum: ulna | Humerus: ulna |
|---|---|---|---|---|---|---|---|---|
| *E. inexpectatus*, holotype | 6.0 | 7.8* | — | 14.9 | 6.5 | 13.6 | 1.74 | 0.77 |
| *E. inexpectatus*, SMNS 80739/3 | — | 8.2 | 6.9 | — | 6.4 | 13.4* | 1.63 | — |
| *Jungornis tesselatus* | 8.0† | 13.0† | — | — | — | 13.8† | 1.06 | 0.62 |
| *Phaethornis pretrei* | 5.6 | 5.9 | 7.7 | 11.7 | 5.2 | 17.8 | 3.02 | 0.95 |
| *Glaucis hirsuta* | 6.0 | 7.3 | 8.4 | 13.2 | 5.2 | 20.2 | 2.77 | 0.82 |
| *Chrysolampis mosquitus* | 4.6 | 6.5 | 6.4 | 10.2 | 4.5 | 15.3 | 2.35 | 0.71 |

*Estimated †Measurements after reference (*7*).